DOI: 10.1111/mice.12745

ORIGINAL ARTICLE

COMPUTER-AIDED CIVIL AND INFRASTRUCTURE ENGINEERING WILEY

A computational framework for finite element modeling of traveling loads on bridges in dynamic regime

Raffaele De Risi

Department of Civil Engineering, University of Bristol, Bristol, UK

Correspondence
Raffaele De Risi, Queen's Building, University Walk, BS8 1TR, Bristol, UK.
Email: raffaele.derisi@bristol.ac.uk

Funding information
EPSRC UKCRIC project, Grant No.: EP/R012806/1

Abstract

The rigorous modeling of traveling loads on bridges in a dynamic regime is not an easy task as the traveling load contributes to the dynamic of the structural system with its mass and damping. In this paper, a simplified approach for traveling loads on bridges in dynamic regime is proposed. The main simplification consists in neglecting the traveling mass. The validity of the proposed simplification is checked with a sensitivity analysis considering a few realistic case-study bridges. The ranges of velocity and traveling-force/bridge-weight ratio are identified. Eventually, the proposed methodology is applied to two case studies, (i) an existing Italian reinforced concrete viaduct and (ii) a pedestrian bridge. The applications show that the proposed simplified approach can be applied to a range of civil engineering problems such as the quantification of the structural reliability of existing structures or the assessment of pedestrian comfort.

1 | INTRODUCTION

The delivery and the maintenance of resilient and sustainable transportation infrastructure are the main priorities of our times (Adeli, 2002), as they are fundamental for the economic development of our nations. Bridges represent the most vulnerable parts of transport infrastructure; without bridges, the transportation network will become a series of disconnected links that will be of little value to the public. Many recent catastrophic events (Figure 1) demonstrated the vulnerability of bridges to the effects of wear-and-tear due to the vehicular traffic. The collapse in 2018 of the Morandi bridge (Calvi et al., 2019; Domaneschi et al., 2020; Malomo et al., 2020) that killed 43 people is only the last event that set off warnings across Europe about aging infrastructure and emphasized the need for new inspections, better record-keeping, and more investment. Among other aspects, a simple manner of modeling the effects of traffic on bridges is now imperative to have a clearer picture of the status of the bridge health with the time (Ng et al., 2009; Scott et al., 2008). As urban areas increase exponentially, increasingly larger vehicles are manufactured, and freight traffic boosts, bridges are subjected to larger and heavier loads. Therefore, dynamic vehicle-bridge interaction (VBI; Brady et al., 2006; Broquet et al., 2004; Dahlberg, 1984; Kim et al., 2005; Li et al., 2008; Senthilvasan et al., 1997; Tan et al., 1998) can no longer be neglected similarly to what has been done for railways bridges (Dimitrakopoulos & Zeng, 2015; Guo et al., 2012; Majka & Hartnett, 2008; Majka & Hartnett, 2009; Ruge et al., 2009; Yang & Yau, 1997; Zhu et al., 2018).

On the other hand, the typical approach to represent traffic loads (Calgaro, 1998; CEN, 2003) is to perform static analyses where the three-dimensional (3D) effects are approximated using geometric distribution factors (Courbon, 1976) and dynamic effects are considered using amplification factors (Caprani et al., 2012; Da Silva, 2004; Deng et al., 2015; González et al., 2008, 2011; Li et al., 2006).

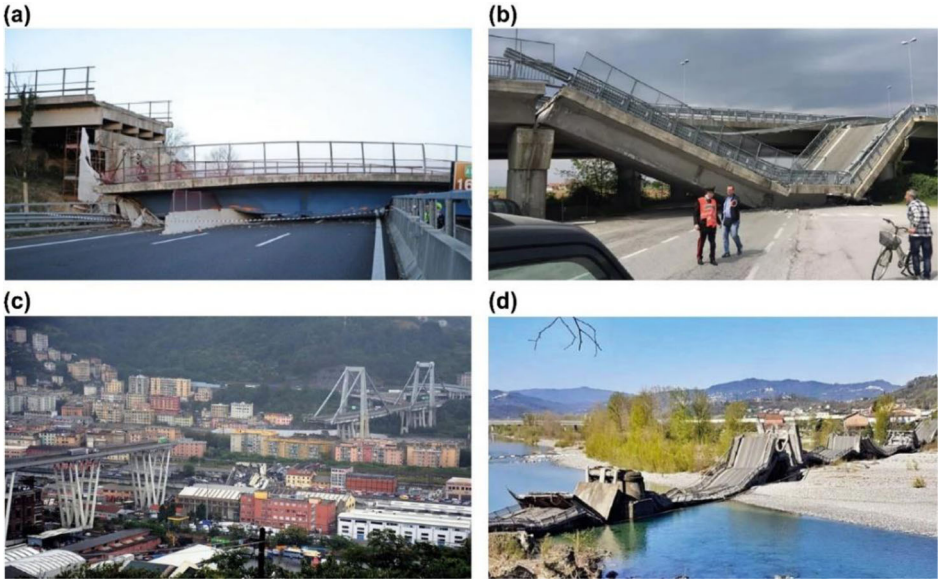

FIGURE 1 (a) October 28, 2016, Lecco overpass collapse (Italy); (b) March 9, 2017, Camerano overpass collapse (Italy); (c) August 14, 2018, Morandi bridge collapse, Genoa (Italy); (d) April 8, 2020, Caprigliola bridge on the Magra river, Caprigliola (Italy)

Loads are usually applied along the bridge on specific locations maximizing the effects according to influence line diagrams (Adeli & Ge, 1989; Adeli & Mak, 1990). These simple deterministic analyses may not be suitable anymore for the assessment of existing bridges since they neglect either the randomness of the traffic flow, that is inherently stochastic (Adeli & Balasubramanyam, 1987; Lipari et al., 2017) for both frequency (Crespo-Minguillón & Casas, 1997) and magnitude of the loading (OBrien et al., 2009) and the dynamic interaction between vehicle and bridge. Also, conventional VBI is modeled with sets of linear differential equations of motion (Zhu et al., 2015) and solved with a variety of methods such as direct integration (Henchi et al., 1998), integration in the frequency domain (Green & Cebon, 1994), the Lagrangian approach (Kim et al., 2005), the pseudo excitation method (Lu et al., 2009), the frequency domain spectral element method (Kim & Lee, 2017), or iterating between the dynamic of the vehicle and the bridge (Zhang & Xia, 2013). It is rare to see the problem solved with finite element analysis software since such an application is still a challenge, especially for the nonlinear behavior (Akin & Mofid, 1989; Azam et al., 2013; Ju et al., 2006; Kidarsa et al., 2008; Kwasniewski et al., 2006; Lin & Trethewey, 1990; Rieker & Trethewey, 1999).

This paper presents a simplified computational framework to model traffic loads on bridges in a dynamic regime that can be implemented/integrated into linear and nonlinear analyses using structural finite element codes, for example, OpenSees (McKenna, 2011; McKenna et al., 2010), SAP2000 (Wilson & Habibullah, 1997); MIDAS (MIDAS, 2020); or developing specific object-oriented classes (Yu & Adeli, 1993) finalized at an optimal bridge

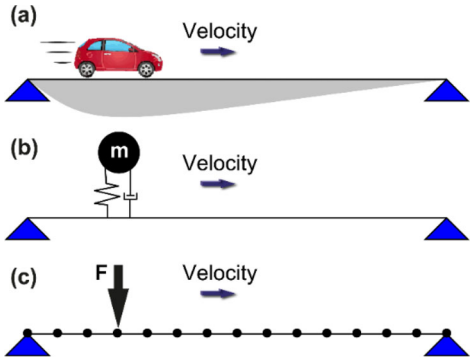

FIGURE 2 (a) Vehicle crossing a bridge; (b) traveling single degree of freedom SDOF/dashpot; (c) traveling massless load

design (Adeli & Balasubramanyam, 1988a, 1988b). Specifically, the path of the generic vehicle is discretized and converted in force-time histories acting on specific locations of the structural model for specific time windows (Chen & Wu, 2011). The main simplification is the modeling of the traveling load (Figure 2a) as a simple traveling massless force in a dynamic regime (Figure 2c). Strictly, as shown in Figure 2b, any traffic load should be modeled as a traveling force, a system of masses, and dashpots (Alexander & Kashani, 2018; Frýba, 2013). To study the effect of such a simplification, a few case-study bridges are analyzed numerically and compared with the analytical solutions provided by Frýba (2013). Once the effects of such a simplification are described and discussed, two applications of the proposed method are presented.

First, an existing Italian reinforced concrete highway bridge is examined, and the results for a single simply supported span are presented and discussed.

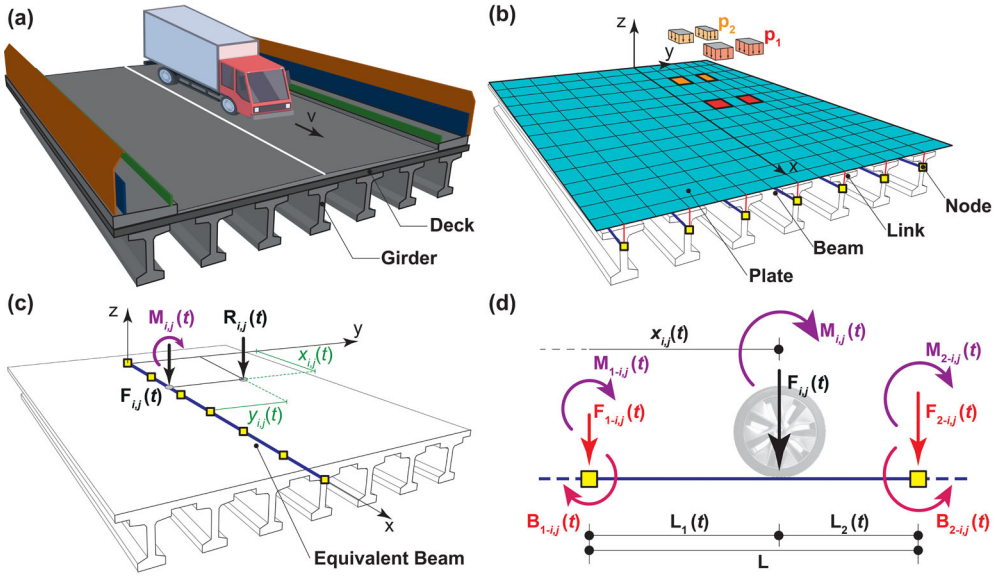

FIGURE 3 (a) Vehicle crossing a bridge with a velocity v; (b) comprehensive modeling of the bridge with plates and beam elements; (c) equivalent beam modeling approach and equivalent force system for a single wheel; (d) equivalent force system for a force acting between two nodes

Second, to demonstrate the versatility of the proposed methodology, an application to the case of pedestrian comfort for a simple pedestrian bridge is also presented.

2 | METHODOLOGY

This section presents how to model a traveling massless load along a bridge in any structural code that allows a dynamic analysis. The algorithm is straightforward and can be implemented for different structural modeling approaches. There are three main points about the implementation of a traveling load in a dynamic regime: (a) position, (b) intensity, and (c) duration. In fact, in general, it is required to define where the load is applied (e.g., concentrated nodal load, uniform pressure), the intensity of the load, and finally a function of time (i.e., a time history) that defines how and how long the load is applied. Figure 3 shows some details elaborated more in the following.

2.1 | Load position

First, consider a generic vehicle crossing a bridge with a given velocity profile $v(t)$ along any possible allowed path (e.g., lane following, Figure 3a). Knowing the trajectory and the velocity profile of the vehicle, it is possible to determine its exact position $[x(t), y(t)]$ on the bridge at any generic time t; where $x(t)$ and $y(t)$ are the positions along the bridge longitudinal and transversal axes, respectively.

If the geometry of the vehicle is also known (e.g., axle spacing (AS) , total vehicle length) then the exact location of each axle and wheel can be calculated as a function of time $[x_{1,1}(t), y_{1,1}(t), x_{1,2}(t), y_{1,2}(t), \ldots, x_{i,j}(t), y_{i,j}(t), \ldots, x_{N,2}(t), y_{N,2}(t)]$; where the subscripts i,j represent the axle number (i) and the wheel number (j), respectively, and N is the total number of axles. Each wheel (movable support) can now be converted into a load on the structural system. The typology of load depends on the type of structural modelling of the bridge. For example, if the bridge is modelled in a very comprehensive manner using 1D or 2D finite elements, or a combination of them (Figure 3b), then a load of each wheel can be modelled either as a uniform vertical pressure load on the plates or as nodal forces on the nodes under the wheel footprint. If more simplified approaches are adopted, for example, the equivalent beam (Figure 3c), then each wheel becomes a force $F_{i,j}(t)$ and a torque $M_{i,j}(t)$ on the beam.

2.2 | Loading system

For the sake of simplicity, in the following, the description of the methodology will focus on the equivalent beam case only. The beam needs to be discretized with multiple nodes along the longitudinal axis. The discretization of the structural system can be studied with a sensitivity analysis in order to achieve the best trade-off between precision and computational effort; such discretization is needed for both refined and simplified modelling approach. Let $R_{i,j}(t)$ be the force applied by the wheel j of the axle i in the

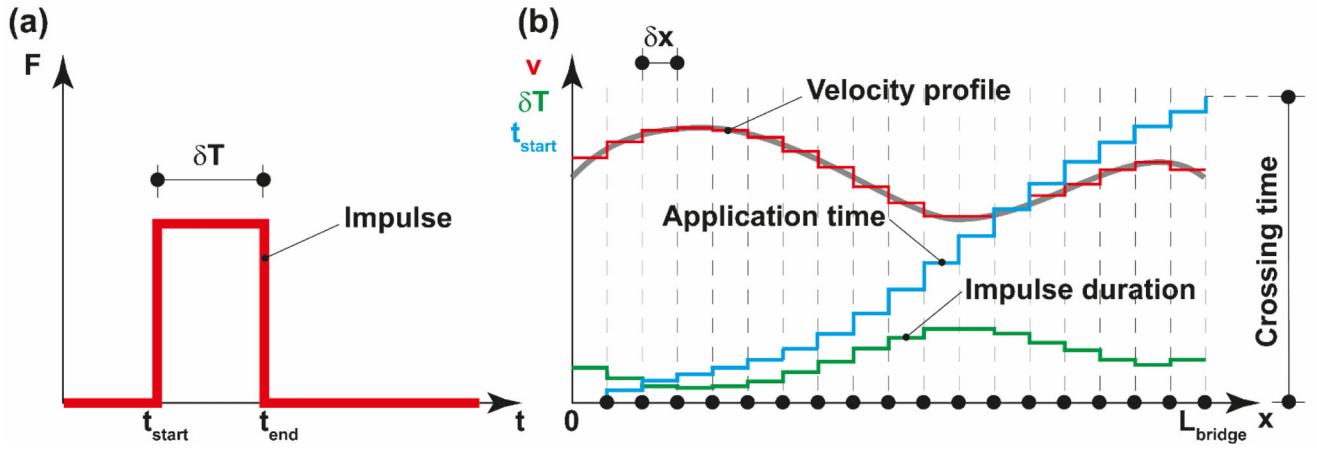

FIGURE 4 (a) Loading function; (b) velocity profile, longitudinal axis arbitrary discretization (different from the finite element discretization), impulse duration, and application time

position $[x_{i,j}(t), y_{i,j}(t)]$. The force system equivalent to $R_{i,j}(t)$ acting on the beam is composed of a force $F_{i,j}(t)$ identical to $R_{i,j}(t)$ and of a torque $M_{i,j}(t) = R_{i,j}(t) \cdot y_{i,j}(t)$ (Figure 3c). At the generic time t, if the force and the torque act at the same position $x_{i,j}(t)$ of any node, they can be applied directly as concentrated loads on the specific node. If the actions are in between the location of two consecutive nodes, a further equivalent force system needs to be defined on the two closest nodes, that is, the previous and the next, with respect to the location of the wheel (Figure 3d). The percentage of force and torque on the two nodes can be calculated as the reactions on a beam fixed at both ends or of a simply supported beam. In the last case, in Figure 3d, $F_{1\text{-}i,j}(t)$ and $M_{1\text{-}i,j}(t)$ are $L_2(t)/L$ times $F_{i,j}(t)$ and $M_{i,j}(t)$, respectively. Analogously, $F_{2\text{-}i,j}(t)$ and $M_{2\text{-}i,j}(t)$ are $L_1(t)/L$ times $F_{i,j}(t)$ and $M_{i,j}(t)$, respectively. The terms $B_{1\text{-}i,j}(t)$ and $B_{2\text{-}i,j}(t)$ are the moments associated with the transport of $F_{1\text{-}i,j}(t)$ and $F_{2\text{-}i,j}(t)$, respectively.

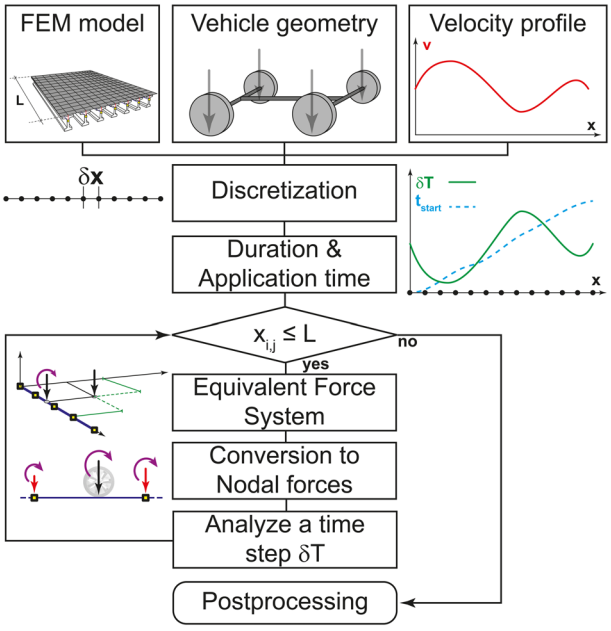

FIGURE 5 Methodology flow-chart

2.3 | Loading function

The last aspects that need to be specified are the duration of the load on each node and the functional form of the load intensity with time. For velocity values that are typical for conventional vehicles (e.g., cars, buses, lorries), a suitable functional form is the pulse function, for which the load increases suddenly to the full value and then goes suddenly to zero after a given duration. A pulse function simplifies the implementation in the loading procedure, and it simplifies the application in structural analysis software.

For a comprehensive definition of the impulse, both impulse duration (δT) and the initial time of application (t_{start}) need to be defined (Figure 4a). To this aim, the best approach is to discretize the longitudinal axis with a very small increment (δx, Figure 4b). It is worth noting that this discretization is different from the discretization of the finite element model. This discretization can be used to evaluate the velocity for each location on the bridge axis, that is, the red line in Figure 4b.

Therefore, the impulse duration can be now calculated as the ratio between δx and the velocity $v(t)$, that is, the green line in Figure 4b. Finally, the application time (t_{start}) can be calculated as the cumulative of the impulse duration, that is, the blue line in Figure 4b.

2.4 | Practical implementation

Figure 5 shows the flowchart for the practical implementation of the methodology. The first step is to build a finite

element model with any of the preferred software platforms. The model can have any level of sophistication. Subsequently, a discretization of the longitudinal axis needs to be carried out (δx); this discretization can be different from that of the finite element model, and it is necessary for the definition of the load in space and time. Second, given the velocity profile of the vehicle, it is possible to derive the application time (t_{start}) and the duration of the impulse (δT) as explained in Section 2.3. Finally, with a for-loop along the discretized longitudinal axis, it is possible to apply the load as an impulse with a given starting time and given duration. If the model is a simple beam, during the for-loop, the force applied by the wheel $R_{i,j}(t)$ is first converted to $F_{i,j}(t)$ and $M_{i,j}(t)$ on the longitudinal axis, and these latter are then converted to concentrated nodal actions as explained in Section 2.2. If the model is a combination of beams for the girders and plates for the deck, then the action applied by the wheel can directly be converted to a uniform vertical pressure on the plates underneath the wheel, or, alternatively, nodal forces distributed on the nodes of the finite element model according to the same criteria presented in Section 2.2 for the equivalent beam. Eventually, a time step of the dynamic analysis can be performed. The procedure ends when each wheel (support more in general) of the considered vehicle crosses the bridge. If the model is linear, then each wheel can be modeled separately, and the results can be eventually combined together using the superposition principle. If the model is nonlinear, then all the wheels need to be modeled together.

2.5 | Implementation in OpenSees

The procedure presented above can be implemented in many of the commercial structural software; on the other hand, in many of those, there are embedded routines – partially controllable– that allow solving the problem of traveling loads. This section presents how to implement this procedure in OpenSees (McKenna, 2011; McKenna et al., 2010) which is an opensource freeware structural software, and therefore, it offers larger flexibility in its use. Moreover, OpenSees has been largely used to model complicated structural model such as bridge structures (Torbol et al., 2013).

In OpenSees, after the definition of the mechanical, geometrical, and inertial characteristics of the model, it is necessary to define a number of "timeSeries Pulse" objects, equal to the number of points with discretization δx (i.e., not the Finite Element Method - FEM - discretization), and an equal number of nodal "pattern Plain" loads associated to each time history defined above. For a complete definition of the pulse time series in OpenSees, a starting time, ending time, and the period of the function need to be defined. The starting time is obtained as explained in Section 2.3; the ending time is obtained adding to the starting time the duration of the impulse derived in Section 2.3; finally, the period can be defined as a number sufficiently larger than the ending time so that it does not change the pulse function.

The damping can be modeled either as Rayleigh damping or as modal damping (Chopra & McKenna, 2016); in both cases, it is convenient to set a small number (e.g., ξ = 0.5%–1%) as the system under traffic load should behave mainly linearly. Moreover, if material nonlinearities are introduced in the model, then it is correct to have a small value of the damping coefficient as the dissipation will be provided by the hysteresis of the materials.

Finally, a transient time-history analysis needs to be defined. The time vector of the transient analysis can be pre-defined considering the minimum ratio $\delta x/v(t)$. The time step can be further reduced to minimize problems associated with large wavenumber transient waves. Simple solution algorithms and integrators can be used for the linear analysis (e.g., Newton, Newmark); more sophisticated ones are needed for nonlinear analyses. In addition, if transient waves remain an issue, to avoid spurious oscillations, smoothed finite element approaches or special time integration techniques can be used (Chai & Zhang, 2020).

3 | NUMERICAL-ANALYTICAL VALIDATION

The numerical approach defined above is here validated against the analytical formulation provided by Frýba (2013). Specifically, three case studies are considered (Figure 6), two reinforced concrete bridges (RC1 and RC2) and one composite steel-reinforced-concrete composite bridge (C); all three bridges are representative of typical simply supported highways overpass. Figure 6a and b show reinforced concrete structural schemes that are generally used for spans up to 25 and 35 m, respectively. Figure 6c shows a composite structural scheme that is used for spans up to 35 m.

For the numerical validation, these three case studies are modeled as equivalent beams; this will allow the comparison with the available analytical solutions. The mechanical and geometrical properties of the three equivalent cross-sections for the three beams are listed in Table 1. The first vibration period (T) of the three case-study bridges is calculated as explained in Appendix A and is shown in Figure 7 for a range of bridge spans (L). The plausible range in Figure 7 is obtained enveloping the empirical data from Paultre et al. (1992). The frequencies ($f = 1/T$) are compared with literature values and an empirical formulation available in the literature (i.e., $f = 82L$–0.9; Paultre et al.,

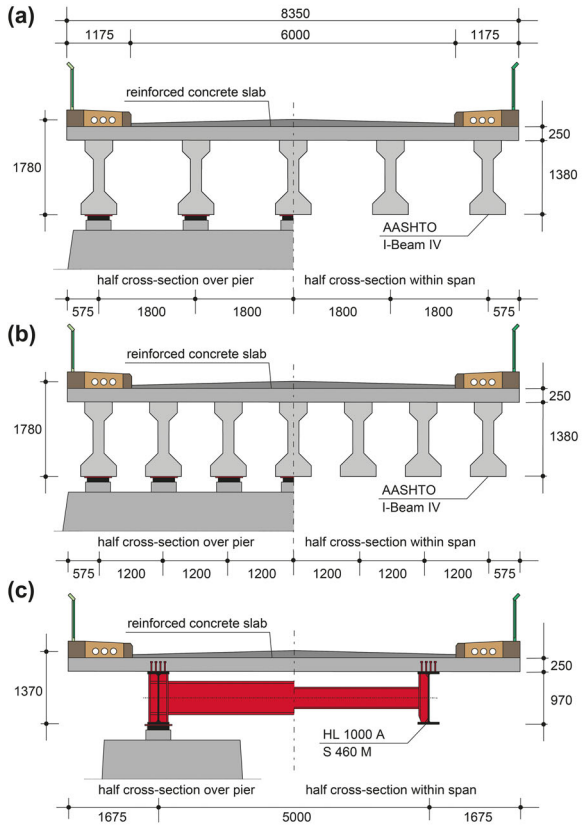

FIGURE 6 Case studies: typical highways' overpasses. (a) RC1: Reinforced concrete structure with span up to 25 m; (b) RC2: reinforced concrete structure with span between 25 and 35 m; (c) C: steel-reinforced concrete composite structure with span up to 35 m

1992; Tilly, 1986). It can be observed that the three bridges are close to the empirical prediction; specifically, the reinforced concrete bridges and the composite bridge are closer to the upper bound and lower bound of the observed vibration frequency variability, respectively. The composite bridge has a systematic lower vibration frequency with respect to the reinforced concrete bridges for the entire range of investigated span values.

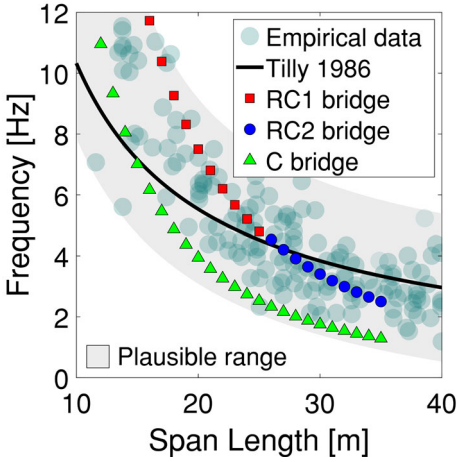

FIGURE 7 Fundamental frequencies versus span length for the three case-study bridges compared to empirical literature data and formulation (Paultre et al., 1992)

Figure 8 shows the comparison between the analytical solutions proposed by Frýba (2013) for a traveling load/load-mass on a simply supported beam (see Appendix B) and the numerical solution for a traveling load proposed in this study solved with OpenSees. The results that can be used to identify the velocity leading to resonance are provided in terms of maximum mid-span displacement as a function of the nondimensional traveling velocity of the force.

It is worth emphasizing that the analytical results used in this study are employed only for the sake of validation of the proposed approach; they are valid only for elastic simply supported beams. The proposed procedure can also be used for the nonlinear problems and for more complicated FEM.

The comparison is provided for the RC1 bridge having a span length of 25 m and for two possible values of traveling force corresponding to 5% and 25% of the total weight of the bridge. It is possible to observe that the OpenSees

TABLE 1 Mechanical and geometrical properties of the three bridges

	RC1	RC2	C
E_c (MPa)	35,220	35,220	35,220
E_s (MPa)	–	–	210,000
ν_c (–)	0.2	0.2	0.2
ν_s (–)	–	–	0.3
γ_c (kN/m^3)	25	25	25
γ_s (kN/m^3)	–	–	78.5
A_{eq} (mm^2)	4,648,460	5,672,844	416,323
$I_{x,eq}$ (mm^4)	30,212,179,398,415	34,638,848,823,700	2,498,167,855,797
$I_{y,eq}$ (mm^4)	1,437,456,752,550	1,787,208,757,822	43,298,103,758
$J_{t,eq}$ (mm^4)	158,823,497,926	204,265,661,221	6,851,245,560
Mass (t/m)	13.85	16.50	9.00

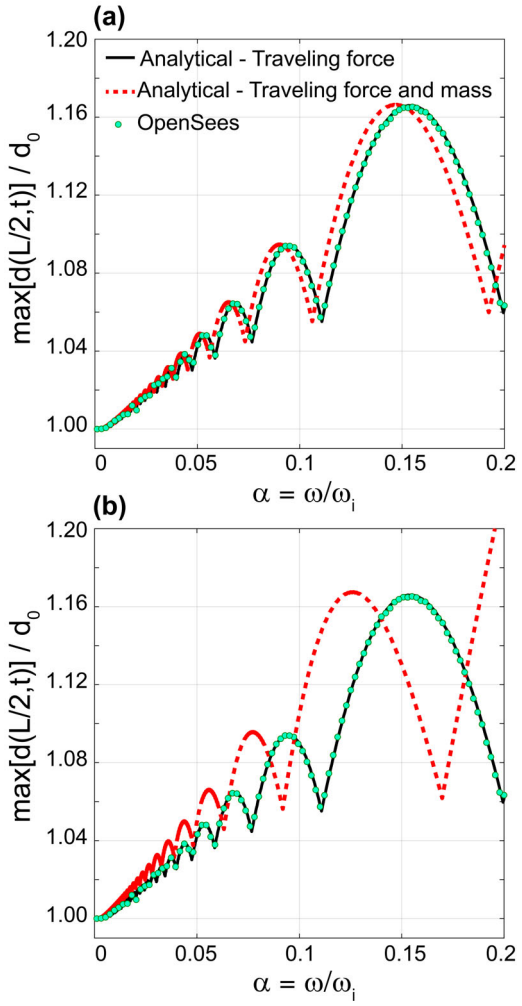

FIGURE 8 Dynamic amplification factor for the mid-span displacement of a simply supported beam for a range of non-dimensional velocity (a) and for a traveling force equal to (a) 5% and (b) 25% of the weight of the bridge, respectively

results (i.e., the green markers) are perfectly aligned with the expected analytical solutions for a traveling force (i.e., the black solid lines); however, both the analytical and numerical results for the simple traveling force are quite different with respect to the case of traveling force and mass (i.e., the red dashed lines). Such a difference increases for increasing force values. To study such a difference, in this work, a sensitivity analysis is also presented for the three considered case-study bridges. Specifically, the ratio between the maximum mid-span displacements obtained considering a traveling force-mass, and only a traveling force is studied. This ratio is studied for a range of bridge spans, for a range of velocities, and a range of values of the traveling force expressed as a percentage of the total bridge weight. Figure 9 shows the results of such a sensitivity analysis.

Specifically, Figure 9a–c show the sensitivity analysis results for the bridges RC1, RC2, and C, respectively, for a span length of 25 m. Figure 9d and e show the results for the bridge RC2 and C, respectively, for a span length of 35 m. For the latter span length, the bridge RC1 is not studied as its maximum span is 25 m. It can be observed that the maximum mid-span displacement due to a traveling force and mass can vary from 90% (de-amplification) to 140% (amplification) of the mid-span displacements obtained for a traveling force only. On the contour plots, the contour line corresponding to 110% is overlayed as a black tick line. Such a value is considered as the limit above which the approximation of a simple traveling force is not acceptable anymore. For all the investigated cases, the limit is exceeded when the force exceeded approximately 30% of the weight of the bridge. Moreover, the limit is a function of the traveling velocity; specifically, the limit is exceeded for lower traveling velocities if the bridge is more deformable, that is, longer for the same cross-section and C rather than RC for the same span length. This velocity is as low as 70 km/h for a bridge C having a span 35 m long.

From the above parametric analysis, it is possible to conclude that if the combinations of vehicle weight and vehicle velocity are far from the exceedance of the 110% area, then the numerical approach is suitable and proven correct with respect to the analytical solution.

4 | APPLICATIONS

Two applications are presented here. The first application presents the assessment of the traffic-related flexural behavior of an existing Italian Highway bridge built in the 1970s. The second application shows the assessment of the pedestrian comfort for the case of a pedestrian bridge. In both cases, the traffic is generated in a stochastic manner (Xu et al., 2017).

4.1 | Stochastic traffic flow on a highway viaduct

For this application, the Akragas highway viaduct in Sicily, Italy, is considered. The geometry details and the material properties are presented in Scibilia and Giancontieri (2018). The viaduct is about 1.4 km long, and each deck in between two consecutive piers is a simply supported system, 35-m long, composed of three prestressed reinforced concrete girders joined by five transversal coupling beams, two at the two ends, and the others located at one-fourth, one-half, and three-fourth of the span. The presence of the transversal beams ensures the joint torsional behavior of the beams. Figure 10a shows the mid-span

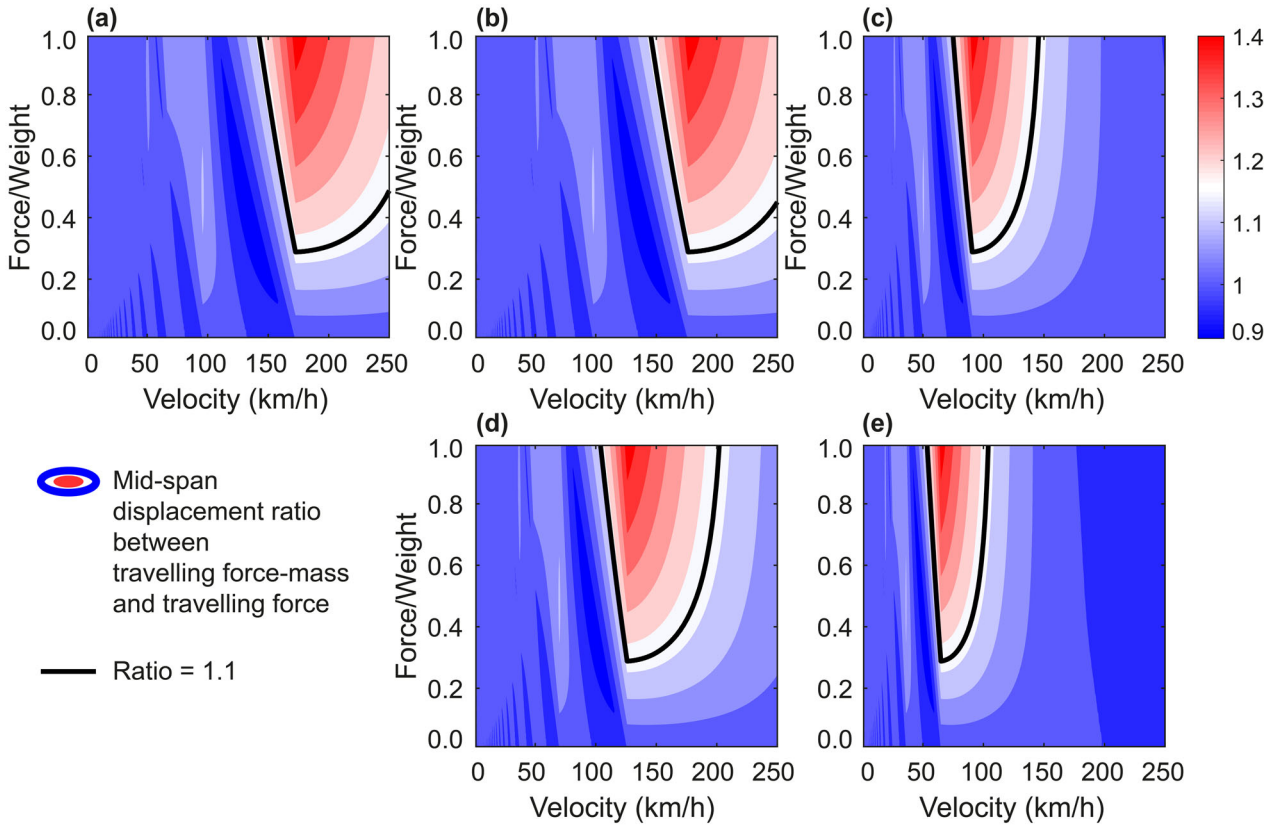

FIGURE 9 Ratio between the mid-displacement obtained considering a traveling mass and force and a traveling force, respectively. (a–c) Results for bridges having 25-m span. (d–e) Results for bridges having 35-m span. (a) Results for the RC1 bridge. (b,d) Results for the RC2 bridge. (d,e) Results for the C bridge

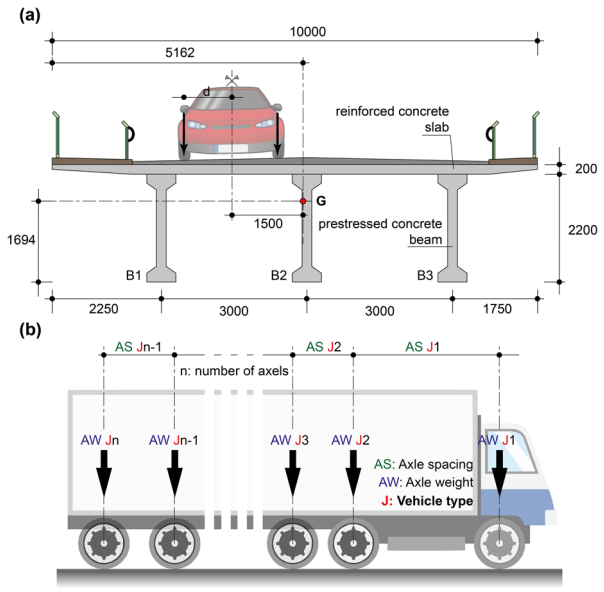

FIGURE 10 (a) Case-study bridge. (b) Weigh-in-motion schematization

TABLE 2 Mechanical ansd geometrical properties of the case-study bridges

	Akragas viaduct	Pedestrian bridge
E_c (MPa)	32,837	31,476
E_s (MPa)	–	210,000
ν_c (–)	0.2	0.2
ν_s (–)	–	0.3
γ_c (kN/m^3)	25	25
γ_s (kN/m^3)	–	78.5
A_{eq} (m^2)	3.788	0.330
$I_{x,eq}$ (m^4)	2.482537	0.13131
$I_{y,eq}$ (m^4)	25.497506	0.34995
$J_{t,eq}$ (m^4)	0.089287	0.16043
Mass (t/m)	10.948	3.179

cross-section of the bridge. Table 2 lists the geometrical and mechanical characteristics of the equivalent beam. The vertical and torsional vibration frequencies calculated according to Appendix A are 3.50 and 1.76 Hz, respectively; the vertical frequency matches very well with the empirical formulation presented in Figure 7. For this example, the bridge is subjected to a traffic flow of 10,000 vehicles on a single lane (i.e., no overtaking is allowed). To simulate the traffic flow, a simulation-based procedure

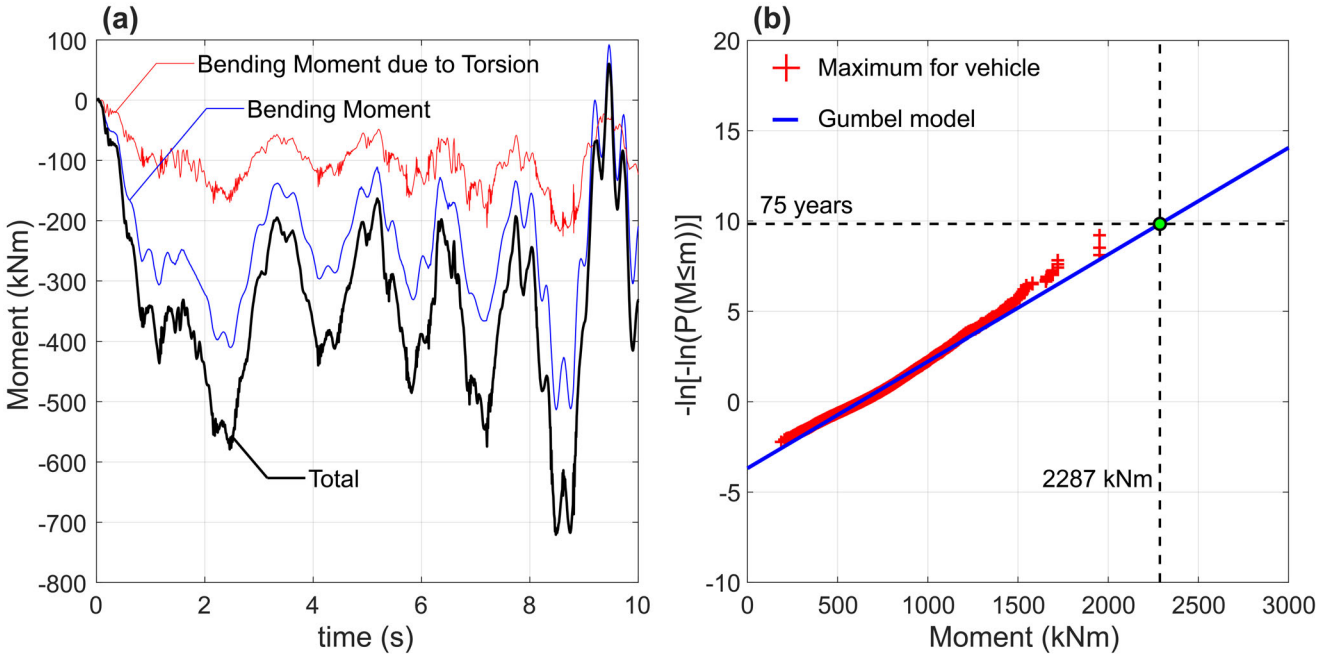

FIGURE 11 (a) 10-s time history of the bending moment of beam B1. (b) Probability paper plot of the maximum (negative) bending moment due to the crossing of 10,000 vehicles

similar to that proposed by Crespo-Minguillón and Casas (1997) is implemented. Simulation-based procedures have been proved very useful to assess existing bridge structures (Chen et al., 2006). Specifically, once the minimum and maximum allowed velocities are defined, the traffic is generated in a stochastic manner, avoiding the collision between two subsequent vehicles (i.e., the inter-vehicle distance, or headway, is always larger than zero).

Together with the simulation of the traffic flow, for each vehicle (Figure 10b), the AS and the axle weight (AW) are simulated using a weigh-in-motion database (WIM) from literature. A WIM database is a repository of vehicle data collected over the years that provide information that can be used to model vehicle actions on infrastructures (Bajwa et al., 2017; Blachowski et al., 2020). In this study, the WIM proposed by Guo et al. (2012) is adopted; in particular, only the vehicle with two and three axels are considered. The database provides with distributions of the AS and AW for the two typologies of vehicles mentioned above. These distributions are used to sample realistic values of loading via a Monte Carlo simulation.

Figure 11 shows the results of the analysis. Specifically, Figure 11a shows the first 10 s of mid-span bending moment for the beam B1 due to only the traffic load (i.e., the total moment is reduced by the quantity associated with the self-weight). Both the total values and the breakdown of the total contribution (see Appendix C) are presented. The biggest contribution to the total moment is due to the total bending moment; the torsion increases values significantly. Figure 11b shows the probability plot of the maximum bending moment in the beam B1 due to the 10,000 vehicles individually. It is possible to observe that the values are distributed according to a Gumble distribution (Enright & O'Brien, 2013), which is generally deemed suitable for describing extreme value data such as traffic-induced stresses.

The fitted Gumble distribution can be used, for example, to identify the bending moment corresponding to a return period of 75 years, that is defied by AASHTO (2012) as a reference for bridges (in this case, 2287 kNm due to traffic only). Moreover, the distribution of loads can be used to solve classical structural reliability problems associated with corrosion or fatigue issues.

4.2 | Pedestrian comfort

To demonstrate the versatility of the proposed procedure, in this example, the application to a pedestrian bridge is presented. Specifically, as a case study, a pedestrian bridge adapted from the SETRA (2006) guidelines is used (Figure 12a). It is a steel box section 40 m-long with a 10 cm concrete deck. The geometrical and mechanical characteristics of the equivalent beam are presented in Table 2. A typical pedestrian crossing the bridge imposes a double-step loading (Figure 12b) that has been widely studied in the literature (Racic et al., 2009). In this study, the undefined shape of the double step is approximated (for the sake

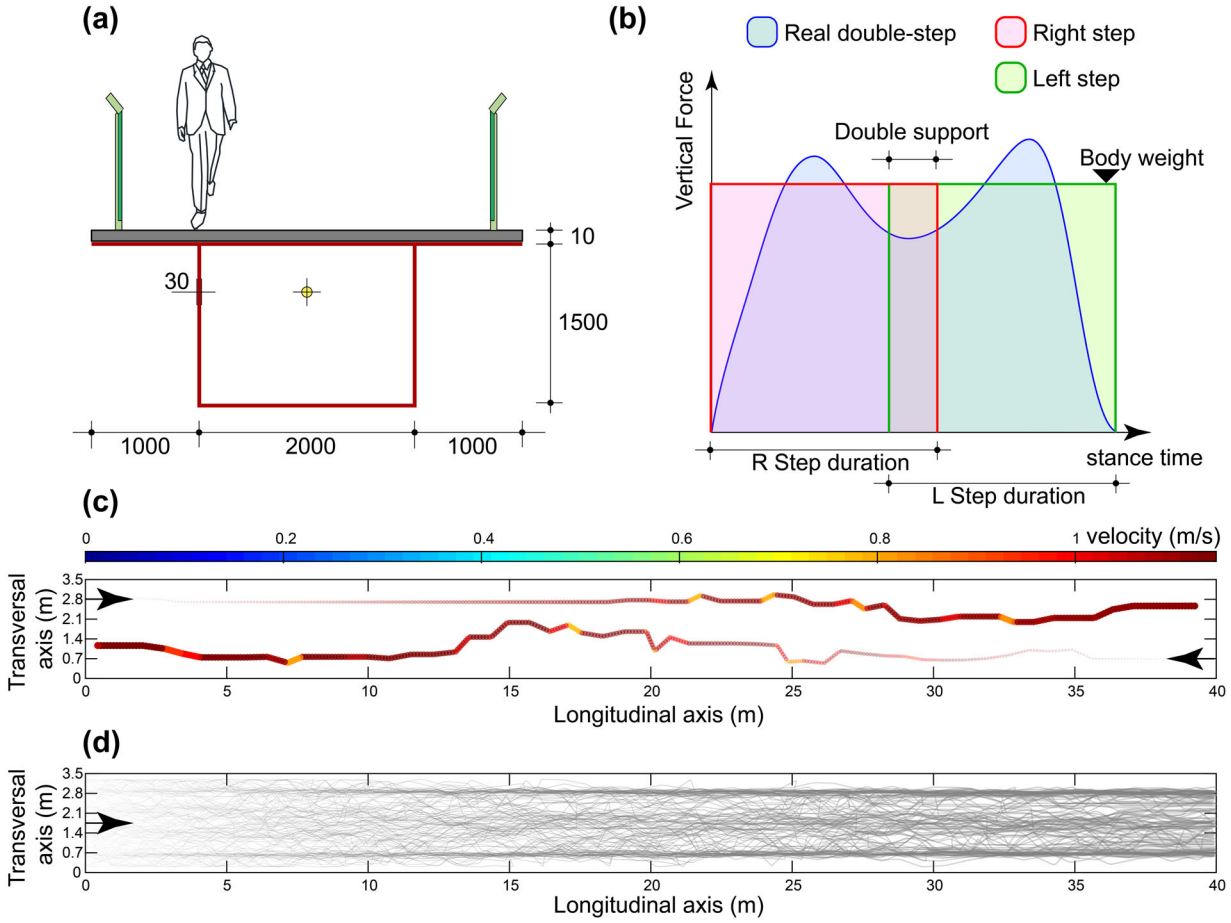

FIGURE 12 (a) Pedestrian bridge cross-section (units in mm). (b) Realistic double-step forcing and its approximation. (c) Example of trajectories from Scenario 1 of two pedestrians crossing the bridge in opposite directions. (d) One-way trajectories of pedestrians from Scenario 2

of simplicity) with two impulses that have a given duration and overlap for a specific time (e.g., 0.15 s). The maximum value of the impulse corresponds with the bodyweight of the pedestrian crossing the bridge. The dynamic loading on the pedestrian bridge can be obtained experimentally (Tian et al., 2019) or simulating potential scenarios of traffic flows using agent-based simulation techniques (Carrol et al., 2012). In this study, two scenarios are simulated using the Vadere crowd simulation tool (Kleinmeier et al., 2019). Simulations are carried out considering a 40×3.5 m aisle. The width of the aisle ($D = 3.5$ m) is smaller than the actual size of the pedestrian bridge due to the presence of the lateral barriers. Two scenarios are considered herein: (a) Scenario 1 (Figure 12c) in which pedestrians move in both directions producing a low-density crowd (i.e., 0.5 pedestrian/m^2), and (b) Scenario 2 (Figure 12d) in which pedestrians move one way from left to right producing a high-density crowd (i.e., 1 pedestrian/m^2). The Vadere tool provides the step time history for each pedestrian; this time history, in combination with the step loading function described above can be used in the methodology proposed in this paper to assess, in a dynamic regime, the vertical acceleration for each point of the structure. Such acceleration values can be used to assess the pedestrian comfort using any available guideline or code (e.g., SETRA, 2006).

Figure 13 shows the results of the simulations. Specifically, the blue line shows the vertical acceleration at the center of the beam, the red line shows the vertical acceleration at D/2 from the center due to the torsional acceleration, and the black line is the sum of the two, therefore presenting the overall peripheric acceleration at D/2 from the center. Figure 13a shows a symmetric profile with maximum acceleration at the beam mid-span. Conversely, Figure 13b shows an asymmetric acceleration profile, skewed toward the right-end; this is consistent with the left-to-right pedestrian flow.

Annexure 2 of Eurocde0 (2002) provides a maximum allowed acceleration value as the limit for the pedestrian comfort of 0.5 m/s^2. According to such a code, it is possible to conclude that pedestrian comfort is guaranteed for both scenarios.

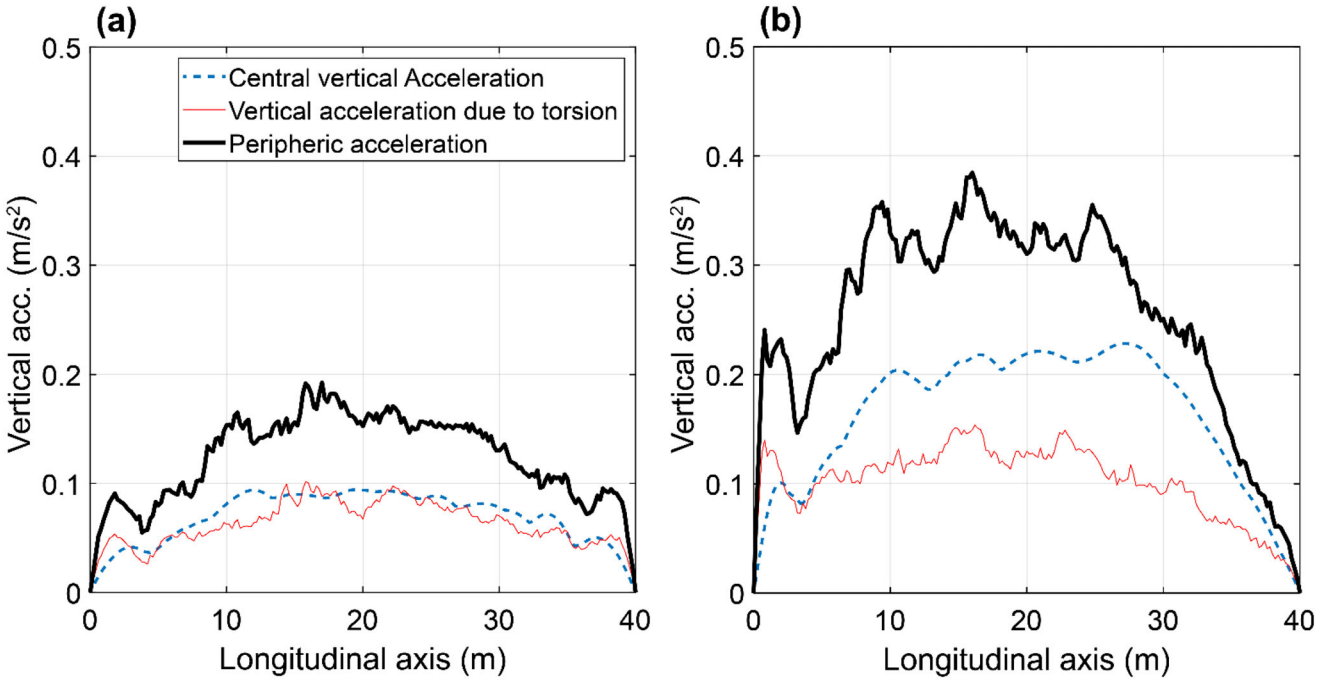

FIGURE 13 Vertical acceleration for (a) Scenario 1 and (b) scenario 2

5 | CONCLUSION

This paper presented a simplified methodology to study bridges under traveling loads in a dynamic regime. The simplification consists of considering the traveling force as a massless vertical pushing system acting on the bridge deck according to a pre-defined time history. The methodological approach consists of the precise definition of the time-dependent position, intensity, and duration of the loads on the structure. The structural model and the loading time histories are then implemented in structural software and solved with a dynamic analysis. In this paper, the implementation in OpenSees was presented.

The simplification of having a simple massless vertical forcing system was investigated with a sensitivity analysis considering three typical bridge deck sections and comparing the numerical results with exact analytical solutions. The main result was that the simplification is valid if the traveling force has an intensity lower than the 30% of the total bridge weight and travels with velocities that are conventional for highways and motorway bridges. This result is consistent with what was observed in Alexander and Kashani (2018).

Two case studies were presented to show the possible applications of the proposed methodology. Both an existing reinforced concrete viaduct and a pedestrian bridge were studied. It was demonstrated that the methodology presented in this paper could be coupled with stochastic traffic simulation procedures in order to derive results that can have several uses such as reliability assessment, fatigue analysis, and pedestrian comfort.

The limitation of this study consists in the lack of further case studies about the application of the proposed methodology to more sophisticated models and nonlinear systems. However, this does not limit the validity of the methodology and can be the subjects of future studies.

ACKNOWLEDGMENTS

This work was carried out using the computational facilities of the Advanced Computing Research Center, University of Bristol (http://www.bris.ac.uk/acrc/). The author was supported by the EPSRC UKCRIC project EP/R012806/1.

REFERENCES

AASHTO (2012). AASHTO LRFD bridge design specification. American Association of State Highway and Transportation Officials.

Adeli, H. (2002). Sustainable infrastructure systems and environmentally-conscious design—A view for the next decade. *Journal of Computing in Civil Engineering*, *16*(4), 231–233.

Adeli, H., & Balasubramanyam, K. V. (1987). A heuristic approach for interactive analysis of bridge trusses under moving loads. *Computer-Aided Civil and Infrastructure Engineering*, *2*(1), 1–18.

Adeli, H., & Balasubramanyam, K. V. (1988a). A knowledge-based system for design of bridge trusses. *Journal of Computing in Civil Engineering*, *2*(1), 1–20.

Adeli, H., & Balasubramanyam, K. V. (1988b). *Expert systems for structural design—A new generation*. Prentice-Hall.

Adeli, H., & Ge, Y. (1989). A dynamic programming method for analysis of bridges under multiple moving loads. *International Journal for Numerical Methods in Engineering*, *28*(6), 1265–1282.

Adeli, H., & Mak, K. Y. (1990). Interactive optimization of plate girder bridges subjected to moving loads. *Computer-Aided Design*, *22*(6), 368–376.

Akin, J. E., & Mofid, M. (1989). Numerical solution for response of beams with moving mass. *Journal of Structural Engineering*, *115*(1), 120–131.

Alexander, N. A., & Kashani, M. M. (2018). Exploring bridge dynamics for ultra-high-speed, hyperloop, trains. *Structures*, *14*, 69–74.

Azam, S. E., Mofid, M., & Khoraskani, R. A. (2013). Dynamic response of Timoshenko beam under moving mass. *Scientia Iranica*, *20*(1), 50–56.

Bajwa, R., Coleri, E., Rajagopal, R., Varaiya, P., & Flores, C. (2017). Development of a cost-effective wireless vibration weigh-in-motion system to estimate axle weights of trucks. *Computer-Aided Civil and Infrastructure Engineering*, *32*(6), 443–457.

Błachowski, B., Świercz, A., Ostrowski, M., Tauzowski, P., Olaszek, P., & Jankowski, Ł. (2020). Convex relaxation for efficient senssor layout optimization in large-scale structures subjected to moving loads. *Computer-Aided Civil and Infrastructure Engineering*, *35*(10), 1085–1100.

Brady, S. P., O'Brien, E. J., & Žnidarič, A. (2006). Effect of vehicle velocity on the dynamic amplification of a vehicle crossing a simply supported bridge. *Journal of Bridge Engineering*, *11*(2), 241–249.

Broquet, C., Bailey, S. F., Fafard, M., & Brühwiler, E. (2004). Dynamic behavior of deck slabs of concrete road bridges. *Journal of Bridge Engineering*, *9*(2), 137–146.

Calgaro, J. A. (1998). Loads on bridges. *Progress in Structural Engineering and Materials*, *1*(4), 452–461.

Calvi, G. M., Moratti, M., O'Reilly, G. J., Scattarreggia, N., Monteiro, R., Malomo, D., Calvi, P. M. & Pinho, R. (2019). Once upon a time in Italy: The tale of the Morandi Bridge. *Structural Engineering International*, *29*(2), 198–217.

Caprani, C. C., González, A., Rattigan, P. H., & OBrien, E. J. (2012). Assessment dynamic ratio for traffic loading on highway bridges. *Structure and Infrastructure Engineering*, *8*(3), 295–304.

Carroll, S. P., Owen, J. S., & Hussein, M. F. M. (2012). Modelling crowd–bridge dynamic interaction with a discretely defined crowd. *Journal of Sound and Vibration*, *331*(11), 2685–2709.

CEN. Comitet Europeen de Normalisation (2003). Eurocode 1: Action on Structures, Part 2: Traffic Loads on Bridges. European Standard EN 1991–2:2003. European Committee for Standardization, Brussels.

Chai, Y., & Zhang, Y. (2020). Transient wave propagation dynamics with edge-based smoothed finite element method and bathe time integration technique. *Mathematical Problems in Engineering*, *2020*, 7180489.

Chen, S. R., & Wu, J. (2011). Modeling stochastic live load for long-span bridge based on microscopic traffic flow simulation. *Computers & Structures*, *89*(9-10), 813–824.

Chen, Y., Feng, M. Q., & Tan, C. A. (2006). Modeling of traffic excitation for system identification of bridge structures. *Computer-Aided Civil and Infrastructure Engineering*, *21*(1), 57–66.

Chopra, A. K., & McKenna, F. (2016). Modeling viscous damping in nonlinear response history analysis of buildings for earthquake excitation. *Earthquake Engineering & Structural Dynamics*, *45*(2), 193–211.

Courbon, J. (1976). Design of multi-beam bridges with intermediate diaphragms: Calculation of multiple beam bridges solidarized by spacers. *Annals of Bridges*, *1976*, 115–116.

Crespo-Minguillón, C., & Casas, J. R. (1997). A comprehensive traffic load model for bridge safety checking. *Structural Safety*, *19*(4), 339–359.

Da Silva, J. G. S. (2004). Dynamical performance of highway bridge decks with irregular pavement surface. *Computers & Structures*, *82*(11-12), 871–881.

Dahlberg, T. (1984). Vehicle-bridge interaction. *Vehicle System Dynamics*, *13*(4), 187–206.

Deng, L., Yu, Y., Zou, Q., & Cai, C. S. (2015). State-of-the-art review of dynamic impact factors of highway bridges. *Journal of Bridge Engineering*, *20*(5), 04014080.

Dimitrakopoulos, E. G., & Zeng, Q. (2015). A three-dimensional dynamic analysis scheme for the interaction between trains and curved railway bridges. *Computers & Structures*, *149*, 43–60.

Domaneschi, M., Pellecchia, C., De Iuliis, E., Cimellaro, G. P., Morgese, M., Khalil, A. A., & Ansari, F. (2020). Collapse analysis of the Polcevera viaduct by the applied element method. *Engineering Structures*, *214*, 110659.

Enright, B., & O'Brien, E. J. (2013). Monte Carlo simulation of extreme traffic loading on short and medium span bridges. *Structure and Infrastructure Engineering*, *9*(12), 1267–1282.

Eurocode0. (2002*). EN 1990: 2002—Basis of structural design*. British Standard Institution.

Frýba, L. (2013). *Vibration of solids and structures under moving loads* (Vol. 1). Springer Science & Business Media.

González, A., Cantero, D., & OBrien, E. J. (2011). Dynamic increment for shear force due to heavy vehicles crossing a highway bridge. *Computers & Structures*, *89*(23-24), 2261–2272.

González, A., Rattigan, P., OBrien, E. J., & Caprani, C. (2008). Determination of bridge lifetime dynamic amplification factor using finite element analysis of critical loading scenarios. *Engineering Structures*, *30*(9), 2330–2337.

Green, M. F., & Cebon, D. (1994). Dynamic response of highway bridges to heavy vehicle loads: theory and experimental validation. *Journal of Sound and Vibration*, *170*(1), 51–78.

Guo, T., Frangopol, D. M., & Chen, Y. (2012). Fatigue reliability assessment of steel bridge details integrating weigh-in-motion data and probabilistic finite element analysis. *Computers & Structures*, *112*, 245–257.

Guo, W. W., Xia, H., De Roeck, G., & Liu, K. (2012). Integral model for train-track-bridge interaction on the Sesia viaduct: Dynamic simulation and critical assessment. *Computers & Structures*, *112*, 205–216.

Henchi, K., Fafard, M., Talbot, M., & Dhatt, G. (1998). An efficient algorithm for dynamic analysis of bridges under moving vehicles using a coupled modal and physical components approach. *Journal of Sound and Vibration*, *212*(4), 663–683.

Ju, S. H., Lin, H. T., Hsueh, C. C., & Wang, S. L. (2006). A simple finite element model for vibration analyses induced by moving vehicles. *International Journal for Numerical Methods in Engineering*, *68*(12), 1232–1256.

Kidarsa, A., Scott, M. H., & Higgins, C. C. (2008). Analysis of moving loads using force-based finite elements. *Finite Elements in Analysis and Design*, *44*(4), 214–224.

Kim, C. W., Kawatani, M., & Kim, K. B. (2005). Three-dimensional dynamic analysis for bridge–vehicle interaction with roadway roughness. *Computers & Structures*, *83*(19-20), 1627–1645.

Kim, T., & Lee, U. (2017). Dynamic analysis of a multi-span beam subjected to a moving force using the frequency domain spectral element method. *Computers & Structures*, *192*, 181–195.

Kleinmeier, B., Zönnchen, B., Gödel, M. & Köster, G. (2019). Vadere: An open-source simulation framework to promote interdisciplinary understanding. Collective Dynamics, [S.l.], v. 4, p. 1–34, ISSN 2366–8539.

Kwasniewski, L., Li, H., Wekezer, J., & Malachowski, J. (2006). Finite element analysis of vehicle–bridge interaction. *Finite Elements in Analysis and Design*, *42*(11), 950–959.

Li, H., Wekezer, J., & Kwasniewski, L. (2008). Dynamic response of a highway bridge subjected to moving vehicles. *Journal of Bridge Engineering*, *13*(5), 439–448.

Li, Y., OBrien, E., & González, A. (2006). The development of a dynamic amplification estimator for bridges with good road profiles. *Journal of Sound and Vibration*, *293*(1-2), 125–137.

Lin, Y. H., & Trethewey, M. W. (1990). Finite element analysis of elastic beams subjected to moving dynamic loads. *Journal of Sound and Vibration*, *136*(2), 323–342.

Lipari, A., Caprani, C. C., & OBrien, E. J. (2017). A methodology for calculating congested traffic characteristic loading on long-span bridges using site-specific data. *Computers & Structures*, *190*, 1–12.

Lu, F., Lin, J. H., Kennedy, D., & Williams, F. W. (2009). An algorithm to study non-stationary random vibrations of vehicle–bridge systems. *Computers & Structures*, *87*(3-4), 177–185.

Majka, M., & Hartnett, M. (2008). Effects of speed, load and damping on the dynamic response of railway bridges and vehicles. *Computers & Structures*, *86*(6), 556–572.

Majka, M., & Hartnett, M. (2009). Dynamic response of bridges to moving trains: A study on effects of random track irregularities and bridge skewness. *Computers & Structures*, *87*(19-20), 1233–1252.

Malomo, D., Scattarreggia, N., Orgnoni, A., Pinho, R., Moratti, M., & Calvi, G. M. (2020). Numerical study on the collapse of the Morandi bridge. *Journal of Performance of Constructed Facilities*, *34*(4), 04020044.

McKenna, F. (2011). OpenSees: a framework for earthquake engineering simulation. *Computing in Science & Engineering*, *13*(4), 58–66.

McKenna, F., Scott, M. H., & Fenves, G. L. (2010). Nonlinear finite-element analysis software architecture using object composition. *Journal of Computing in Civil Engineering*, *24*(1), 95–107.

MIDAS, Gen & Civil. Online manuals. MIDAS Information Technology (2020). https://globalsupport.midasuser.com/helpdesk/

Ng, M., Lin, D. Y., & Waller, S. T. (2009). Optimal long-term infrastructure maintenance planning accounting for traffic dynamics. *Computer-Aided Civil and Infrastructure Engineering*, *24*(7), 459–469.

OBrien, E. J., Rattigan, P., González, A., Dowling, J., & Žnidarič, A. (2009). Characteristic dynamic traffic load effects in bridges. *Engineering Structures*, *31*(7), 1607–1612.

Paultre, P., Chaallal, O., & Proulx, J. (1992). Bridge dynamics and dynamic amplification factors—a review of analytical and experimental findings. *Canadian Journal of Civil Engineering*, *19*(2), 260–278.

Racic, V., Pavic, A., & Brownjohn, J. M. W. (2009). Experimental identification and analytical modelling of human walking forces: Literature review. *Journal of Sound and Vibration*, *326*(1-2), 1–49.

Rieker, J. R., & Trethewey, M. W. (1999). Finite element analysis of an elastic beam structure subjected to a moving distributed mass train. *Mechanical Systems and Signal Processing*, *13*(1), 31–51.

Ruge, P., Widarda, D. R., Schmälzlin, G., & Bagayoko, L. (2009). Longitudinal track–bridge interaction due to sudden change of coupling interface. *Computers & Structures*, *87*(1-2), 47–58.

Scibilia, N., & Giancontieri, S. (2018). *The resistance of prestressed beams of the Akragas bridge* (SS 115-AG). http://www.associazioneaicap.com/wp-content/uploads/2018/03/22-SCIRES.pdf

Scott, M. H., Kidarsa, A., & Higgins, C. (2008). Development of bridge rating applications using OpenSees and Tcl. *Journal of Computing in Civil Engineering*, *22*(4), 264–271.

Senthilvasan, J., Brameld, G. H., & Thambiratnam, D. P. (1997). Bridge–vehicle interaction in curved box girder bridges. *Computer-Aided Civil and Infrastructure Engineering*, *12*(3), 171–182.

SÉTRA (2006). *Technical guide, footbridges: Assessment of vibrational behaviour of footbridges under pedestrian loading*. Service d'Etudes techniques des routes et autoroutes.

Tan, G. H., Brameld, G. H., & Thambiratnam, D. P. (1998). Development of an analytical model for treating bridge-vehicle interaction. *Engineering Structures*, *20*(1-2), 54–61.

Tian, Y., Zhang, J., & Yu, S. (2019). Rapid impact testing and system identification of footbridges using particle image velocimetry. *Computer-Aided Civil and Infrastructure Engineering*, *34*(2), 130–145.

Tilly, G. P. (1986). Dynamic behaviour of concrete structures. Report of the Rilem 65MDB Committee: Developments in civil engineering (Vol. 13). Elsevier.

Torbol, M., Gomez, H., & Feng, M. (2013). Fragility analysis of highway bridges based on long-term monitoring data. *Computer-Aided Civil and Infrastructure Engineering*, *28*(3), 178–192.

Wilson, E. L., & Habibullah, A. (1997). *SAP2000 integrated finite element analysis and design of structures*. Berkeley, California: Computers and Structures Inc.

Xu, J., Spencer, B. F., Lu, X., Chen, X., & Lu, L. (2017). Optimization of structures subject to stochastic dynamic loading. *Computer-Aided Civil and Infrastructure Engineering*, *32*(8), 657–673.

Yang, Y. B., & Yau, J. D. (1997). Vehicle-bridge interaction element for dynamic analysis. *Journal of Structural Engineering*, *123*(11), 1512–1518.

Yu, G., & Adeli, H. (1993). Object-oriented finite element analysis using EER model. *Journal of Structural Engineering*, *119*(9), 2763–2781.

Zhang, N., & Xia, H. (2013). Dynamic analysis of coupled vehicle–bridge system based on inter-system iteration method. *Computers & Structures*, *114*, 26–34.

Zhu, D. Y., Zhang, Y. H., & Ouyang, H. (2015). A linear complementarity method for dynamic analysis of bridges under moving vehicles considering separation and surface roughness. *Computers & Structures*, *154*, 135–144.

Zhu, Z., Gong, W., Wang, L., Li, Q., Bai, Y., Yu, Z., & Harik, I. E. (2018). An efficient multi-time-step method for train-track-bridge interaction. *Computers & Structures*, *196*, 36–48.

How to cite this article: De Risi R. A computational framework for finite element modeling of traveling loads on bridges in dynamic regime. *Comput Aided Civ Inf*, 2021;1–15. https://doi.org/10.1111/mice.12745

APPENDIX A

The *i*th translational vibration period of a simply supported beam having span length L and distributed mass μ is calculated as follows:

$$T_i = \left(\frac{L}{i}\right)^2 \frac{2}{\pi}\sqrt{\frac{\mu}{EI}} \tag{A.1}$$

where E is the beam Young's modulus, and I is the constant moment of inertia of the cross-section of the beam.

The *i*th torsional vibration period is calculated as follows:

$$T_i = \frac{2}{n} L^2 \sqrt{\frac{\rho I_0}{L^2 G J_{t,\mathrm{eq}}}} \tag{A.2}$$

where ρ is the density, I_0 is the polar moment of inertia, G is the elastic shear modulus, and $J_{\mathrm{t,eq}}$ is the torsion constant. According to the perpendicular axis theorem, I_0 can be calculated as the sum of the moment of inertia $I_{x,\mathrm{eq}}$ and $I_{y,\mathrm{eq}}$.

APPENDIX B

With reference to Figure 2c and according to Frýba (2013) the mid-span displacement for a simply supported beam crossed by a traveling load having constant speed v acting at time t on the position x is:

$$d\ (x,t) = d_0 \sum_{i=1}^{\infty} \frac{1}{i^2\left[i^2(i^2-\alpha^2)^2 + 4\alpha^2\beta^2\right]} \times \left\{ i^2\left(i^2-\alpha^2\right)\sin(i\omega t) - \frac{i\alpha\left[i^2\left(i^2-\alpha^2\right)-2\beta^2\right]}{\left(i^4-\beta^2\right)^{\frac{1}{2}}} e^{-\omega_b t}\sin\left(\omega_i' t\right) - 2i\alpha\beta\left[\cos(i\omega t) - e^{-\omega_b t}\cos\left(\omega_i' t\right)\right] \right\} \times \sin\left(\frac{i\pi x}{L}\right) \tag{B.1}$$

where x is the length coordinate, L is the length of the beam, t is the time coordinate starting at the instant the force arrives on the beam, d_0 is the mid-span deflection of a simply supported beam loaded with a force F at point $x = L/2$:

$$d_0 = \frac{FL^3}{48EI} \tag{B.2}$$

where E is the beam Young's modulus and I is the constant moment of inertia of the cross-section of the beam. Moreover, in Equation (B.1), i is the number of the vibration mode, and α and β are the two dimensionless parameters:

$$\alpha = \frac{\omega}{\omega_i} \quad \beta = \frac{\omega_b}{\omega_i} \tag{B.3}$$

where ω is the circular frequency of the loading, ω_i is the circular frequency of the *i*th vibration mode, and ω_b is the circular frequency of damping of the beam:

$$\omega_i = \sqrt{\frac{i^4\pi^4}{L^4}\frac{EI}{\mu}} \quad \omega = \frac{\pi v}{L} \quad \omega_b = \xi\omega_i \tag{B.4}$$

where μ is the constant mass per unit length of the beam, and ξ is the damping ratio. Finally, ω_i' for lightly damped system is equal to:

$$\omega_i' = \sqrt{\omega_i^2 - \omega_b^2} \tag{B.5}$$

Frýba (2013) provides also a simplified solution for a traveling force and mass. The solution is based on the following factor η:

$$\eta = 1 + \frac{2F}{\mu L g}\sin^2\left(\frac{i\pi x_o}{L}\right) \tag{B.6}$$

where x_o is a location of the traveling mass m (each instant considered immobile) and g is the gravity acceleration. The solution for this case is the same as Equation (B.1) where some of the terms are changed as follows:

$$\bar{\omega}_i = \frac{\omega_i}{\sqrt{\eta}} \quad \bar{\omega}_b = \frac{\omega_b}{\eta} \quad \omega_i' = \sqrt{\bar{\omega}_i^2 - \bar{\omega}_b^2} \tag{B.6}$$

and α and β are changed accordingly.

APPENDIX C

This appendix explains how the final bending moment at the midspan of beam B1 for the case study presented in Figure 11a is calculated. Specifically, the bending moment acting on the beam B1 is:

$$M_{B1} = \frac{m_F}{3} + \frac{V}{2}\frac{L}{2} \tag{C.1}$$

where m_F is the bending moment from the analysis (Figure C1) on the equivalent beam, L is the beam span, and V is the additional shear acting on the beam associated with the torsion m_T (Figure C1). V is calculated according to the Courbon (1976) approach:

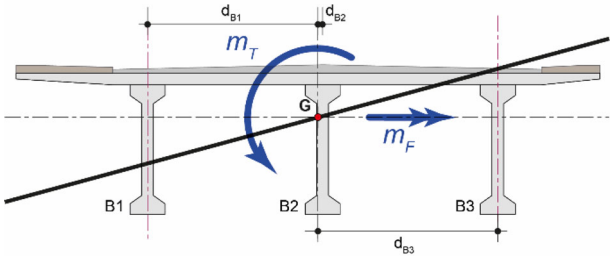

FIGURE C1 Reference scheme

$$V = \frac{m_T}{\left(d_{B1} + \frac{d_{B2}^2}{d_{B1}} + \frac{d_{B3}^2}{d_{B1}}\right)} \tag{C.2}$$

where d_{B1}, d_{B2}, and d_{B3} are the distances between the central axes of the three beams and the axis of the equivalent beam (G in Figure C1).